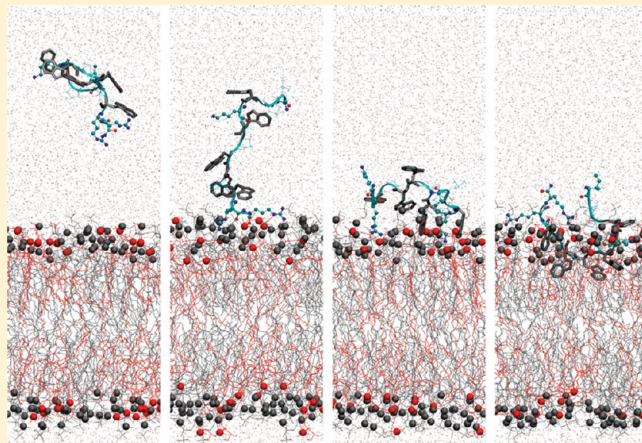


# Free Energy Difference in Indolicidin Attraction to Eukaryotic and Prokaryotic Model Cell Membranes

In-Chul Yeh,\* Daniel R. Ripoll, and Anders Wallqvist

Biotechnology High Performance Computing Software Applications Institute, Telemedicine and Advanced Technology Research Center, U.S. Army Medical Research and Materiel Command, Fort Detrick, Maryland

**ABSTRACT:** We analyzed the thermodynamic and structural determinants of indolicidin interactions with eukaryotic and prokaryotic cell membranes using a series of atomistically detailed molecular dynamics simulations. We used quartz-supported bilayers with two different compositions of zwitterionic and anionic phospholipids as model eukaryotic and prokaryotic cell membranes. Indolicidin was preferentially attracted to the model prokaryotic cell membrane in contrast to the weak adsorption on the eukaryotic membrane. The nature of the indolicidin surface adsorption depended on an electrostatic guiding component, an attractive enthalpic component derived from van der Waals interactions, and a balance between entropic factors related to peptide confinement at the interface and counterion release from the bilayer surface. Thus, whereas we attributed the specificity of the indolicidin/membrane interaction to electrostatics, these interactions were not the sole contributors to the free energy of adsorption. Instead, a balance between an attractive van der Waals enthalpic component and a repulsive entropic component determined the overall strength of indolicidin adsorption.



## INTRODUCTION

Antimicrobial peptides are small cationic peptides that play important roles in the host-defense mechanism of many living organisms against bacterial infections.<sup>1–3</sup> Antimicrobial peptides act rapidly against a broad spectrum of microbes and have attracted attention as potential novel antibiotics to combat multidrug-resistant bacterial infections, either as standalone agents or in combination therapies with other conventional antibiotics.<sup>4–6</sup> Indolicidin is an antimicrobial peptide isolated from bovine neutrophils.<sup>7</sup> It consists of 13 amino acid residues ( $\text{NH}_3^+$ -ILPWKPWPWPWR-NH<sub>2</sub>) with an uncapped N-terminus and an amidated C-terminus resulting in a net positive charge of 4 e. The structure of indolicidin is known to be disordered in aqueous solution but has been shown to form an extended conformation when bound to detergent micelles.<sup>8</sup> The mechanism of indolicidin action against both bacterial and human cells has been investigated both experimentally<sup>9–17</sup> and computationally.<sup>18–20</sup> Even though several different mechanisms of action by indolicidin have been proposed, the exact mechanism remains unclear.<sup>14,20</sup> The delineation of the mechanism is not straightforward because the biological action that ultimately results in lysis of bacteria is multifaceted. Initially, indolicidin must recognize and attach to bacterial cell membranes. After this attachment, several lytic mechanisms are possible, for example, membrane thinning resulting in a structural weakening of the membrane and loss of cell homeostasis, interactions with proteins in the membrane, or translocation to the cytosol where the peptide can further

interact with diverse cellular targets, such as RNA and DNA, or other highly charged species. Existing results from both experimental<sup>8,14,16</sup> and computer simulation<sup>18–20</sup> work confirm that the indolicidin's mechanism of action includes an important localization component associated with peptide adsorption to the solvent side of membrane bilayer interface. In this work, we quantify and address the detailed thermodynamic and structural elements of this initial attraction of indolicidin to model prokaryotic and eukaryotic bilayers using computational approaches.

Solid-supported lipid bilayers are widely used as experimental model systems to investigate detailed interactions of biological molecules with membranes. Such model systems have been used to investigate the interactions of antimicrobial peptides with lipid membranes using quartz crystal microbalance (QCM) measurements,<sup>12,21</sup> sum frequency generation (SFG) vibrational spectroscopy,<sup>22,23</sup> and in situ atomic force microscopy (AFM).<sup>14–16</sup> Similarly, one can use computational models to create realistic solid-supported lipid bilayers at the atomic level<sup>24–27</sup> to map out the interactions of antimicrobial peptides with lipid membranes in great detail. Recently, we successfully modeled solid-supported bilayers with a hydrated dimyristoylphosphatidylcholine (DMPC) lipid bilayer deposited on a quartz crystal surface.<sup>28</sup> Importantly, we showed a

Received: December 9, 2011

Revised: February 10, 2012

Published: February 16, 2012

critical need to implement the appropriate electrostatic boundary conditions for simulations and analyses to capture the structural and electrostatic properties of DMPC lipid bilayers that correspond to the physical systems being modeled, for example, solvated bilayers representing lamellar systems, nonlamellar bilayers mimicking membranes, and quartz-supported bilayers. These methodological considerations are critical because the electrostatic interaction between cationic antimicrobial peptides and the anionic lipids in the bacterial cell membrane is a key feature that governs the selective attraction of antimicrobial peptides to the bacterial cell membrane.<sup>3,29</sup> A detailed understanding of this electrostatic interaction needs to take into consideration all the complex interactions among explicit solvent molecules, counterions, and salt ions present under physiological conditions. In particular, counterions and salts strongly diminish the electrostatic interactions between antimicrobial peptides and anionic lipids, leading to a more nuanced interpretation of the electrostatic effect associated with cationic antimicrobial peptides.

In this work, we investigated the differences in the interaction of the antimicrobial peptide indolicidin with model bacterial and eukaryotic cell membranes by performing atomistically detailed molecular dynamics (MD) simulations that included solvent molecules, salt ions, and lipids. We constructed model prokaryotic and eukaryotic cell membranes using mixed (zwitterionic and anionic) and neutral (zwitterionic) lipid bilayers respectively deposited on a quartz crystal surface. To characterize the interaction of indolicidin with the lipid membranes, we calculated the potential of mean force (PMF)<sup>30</sup> or free energy profile with respect to the distance of indolicidin from the lipid membrane using a series of MD simulations. We confirmed the existence of the selective attractive interaction of indolicidin with the model bacterial cell membrane, which results in indolicidin being preferentially located at the membrane interface. We further characterized the nature of the underlying interaction in terms of structural and thermodynamic properties. In particular, we found that placement of indolicidin at the membrane surface was associated with a minimum PMF of  $-3.5 \pm 0.2$  kcal/mol at the prokaryotic membrane, compared to  $-0.6 \pm 0.6$  kcal/mol at the eukaryotic membrane. We further used the distance-dependent PMF to estimate the free energy of indolicidin adsorption ( $\Delta G^\circ$ ) to be  $-1.94 \pm 0.56$  kcal/mol for the model prokaryotic cell membrane and  $-0.05 \pm 0.46$  kcal/mol for the eukaryotic membrane. The detailed thermodynamic and structural analysis of these systems provided support for the idea that the specificity of the indolicidin/membrane interaction can be attributed to electrostatics, but these interactions were not the sole contributors to the free energy of adsorption. Instead, a balance between an attractive van der Waals enthalpic component and a repulsive entropic component determined the overall strength of indolicidin adsorption.

## METHODS

**Simulations.** MD simulations were performed with the NAMD MD simulation program<sup>31</sup> using the CHARMM 27 all atom force field.<sup>32</sup> We used DMPC and dimyristoyl phosphatidylglycerol (DMPG) as model zwitterionic and anionic phospholipids, respectively. The TIP3P model<sup>33</sup> was used to describe water molecules. The force field for the quartz (011) crystal was taken from one developed by Lopes et al.<sup>34</sup> A primitive unit cell of quartz (011) of  $\sim 15$  Å thickness was

replicated in two dimensions to construct a quartz (011) crystal with a surface area of  $36.5 \times 37.0$  Å<sup>2</sup> in the unit cell, as in the previous study by Lopes et al.<sup>34</sup> and in our recent study.<sup>28</sup> One side of the constructed crystal was covered with hydrophilic silanols (Si–OH), and silicon atoms on the other side were saturated with hydrogens (Si–H). Crystal atoms, except for the O–H groups of silanols, were held fixed to maintain the (011) crystal geometry. Short-range interactions outside a 10 Å cutoff were truncated. Long-range electrostatic interactions were calculated with the particle mesh Ewald method<sup>35</sup> with a correction term for the planar vacuum boundary condition,<sup>28,36</sup> referred to as EW3DC, which we implemented in NAMD. The EW3DC correction term, combined with a sufficiently large box length ( $L_z$ ) in the  $z$  direction normal to the interface, effectively implements a 2D periodic boundary condition, which is appropriate for solid-supported lipid bilayers. Bonds involving hydrogens were constrained with the SHAKE algorithm.<sup>37</sup> We used a time step of 2 fs for the time integration, and the temperature was maintained at 310 K using Langevin dynamics with a damping coefficient of 10 ps<sup>-1</sup>.<sup>38</sup>

### Preparation of Quartz-Supported Lipid Bilayers.

Quartz-supported lipid bilayers were prepared as illustrated in Figure 1. Hydrated lipid bilayers are in contact with the

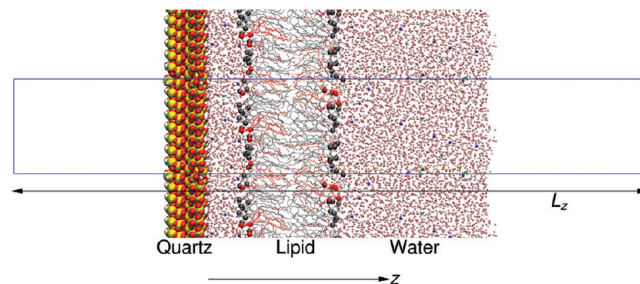


**Figure 1.** Snapshot of the hydrated DMPC/G lipid bilayer supported on a quartz crystal illustrates the placement of the unit cell in the supported bilayer system. The blue box represents the unit simulation cell with an  $L_z$  of 250 Å. The simulation cell is repeated periodically in all three directions. Gray and red lines represent DMPC and DMPG lipids, respectively. Gray and red balls near the membrane interfaces denote phosphorus atoms of headgroups in DMPC and DMPG lipids, respectively. Smaller pink spheres represent oxygen atoms of water molecules. Blue and green spheres represent sodium and chloride ions, respectively.

hydrophilic side of the quartz crystal. Both a pure DMPC bilayer and a mixed DMPC/DMPG (DMPC/G) bilayer were prepared as model eukaryotic and bacterial cell membranes, respectively. For a starting point of a pure DMPC bilayer, we used the last configuration from the 200 ns simulation of the DMPC bilayer composed of 44 DMPC molecules (22 on each leaflet) supported on the quartz surface described in our previous work.<sup>28</sup> Similarly, a mixed lipid bilayer with 34 DMPC and 10 DMPG molecules (17 DMPC and 5 DMPG on each leaflet) supported on the quartz surface was prepared after a 45 ns equilibration in aqueous solution and a 50 ns equilibration on the quartz surface. An initial configuration of the mixed DMPC/G lipid bilayer was prepared with the CHARMM-GUI.<sup>39</sup> In these configurations, the upper water layer between the lipid bilayer and the water/vacuum interface contained about twice as many water molecules as the lower water layer between the bilayer and the quartz. To increase the bulklike region of water to accommodate indolicidin, we doubled the

number of water molecules in the upper water layer. As a result, the upper water layer contains about four times as many water molecules as the lower water layer. To observe the effects of salt ions on the properties of lipid bilayers, we performed simulations with and without added NaCl salt for a pure DMPC bilayer. For a simulation with salt, we added 2 and 8 pairs of NaCl to the lower and upper water layers respectively resulting in a salt concentration of about 0.16 M, commensurate with physiological salt concentrations. For a simulation with the mixed DMPC/G bilayer, 10 extra sodium counterions (5 to each water layer) were added to maintain the net charge neutrality. The area per lipid headgroup is about 60 Å<sup>2</sup>, which is close to the experimental value for DMPC.<sup>40</sup> The box length ( $L_z$ ) in the  $z$  direction normal to the interface was fixed at 250 Å, which was large enough to create a water/vacuum interface as shown in Figure 1. This allowed the system to adjust to an optimum density without the need of constant-pressure simulations. Simulation for each prepared quartz-supported lipid bilayer system lasted 100 ns. The initial 20 ns were discarded as equilibration.

**Preparation of Indolicidin.** Five different initial configurations of indolicidin were prepared. The first configuration was taken from the structure of indolicidin bound to a dodecylphosphocholine (DPC) micelle as determined by NMR (PDB id: 1g89).<sup>8</sup> After a brief energy minimization, we performed an MD simulation of indolicidin in aqueous solution for 100 ns. The other four conformations of indolicidin were selected from conformations generated by the ECEPPAK program.<sup>41,42</sup> We selected two conformations where NOE distances deviated less than 1 Å from experimental values and another two conformations where the C<sub>α</sub> rmsd of the core residues 3–11 was less than 1 Å away from the NMR model structure. We performed an MD simulation lasting 30 ns in aqueous solution for each of the four selected conformations. We kept the last conformation of indolicidin from each solution simulation and placed it in the middle of the upper water layer after removing water molecules within 2.8 Å of the indolicidin peptide. The number of counterions in the upper water layer was adjusted to maintain charge neutrality in the presence of the positively (+4) charged indolicidin.

**Calculation of the Free Energy Profile.** For a detailed understanding of how indolicidin interacts with lipid bilayers, we performed MD simulations with the peptide  $z$  position restrained at various points in the aqueous phase with NAMD's *colvar* module. We used a harmonic biasing potential with a force constant of 2.0 kcal/(mol Å<sup>2</sup>) applied to the center of mass  $z$  position of indolicidin. The  $z$  position bias was implemented at every 1 Å interval from 52 to 96 Å with respect to the quartz surface, and each biased simulation lasted 25 ns. We calculated the free energy or PMF profile by applying the weighted histogram analysis method<sup>43,44</sup> to the last 15 ns of the simulation data. A total of 3.375 μs of the simulation data derived from five different and independent starting configurations were used to calculate the free energy profile for each bilayer system. However, the  $z$  position bias for simulations starting with the NMR model structure was extended up to 125 Å to observe the structural properties of the peptide near the water/vacuum interface.

**Lipid Order Parameter.** The acyl chain lipid order parameter profile<sup>45</sup> is one of the important quantities describing the properties of lipid bilayers. To probe possible disruptions of the membranes caused by indolicidin, we calculated the carbon-deuterium lipid order parameter  $S_{CD}$  for

the aliphatic C–H bond vectors of each carbon atom of the acyl chain  $n=1$  with the following formula:

$$S_{CD} = \left\langle \frac{3\cos^2 \theta - 1}{2} \right\rangle \quad (1)$$

where  $\theta$  is the angle between the C–H vector and the  $z$  axis. The order parameter  $S_{CD}$  is zero for a completely unordered (isotropic) system. A perfectly ordered acyl chain in an all-trans conformation results in an  $S_{CD}$  value of −0.5.<sup>45</sup>

**Electrostatic Property Profiles Across the Interface in Periodic Boundary Conditions.** Distribution of the electric field along the  $z$  direction  $E(z)$  was calculated from the charge density distribution  $\rho_q(z)$  obtained from the simulations using the following relationship:<sup>28,36,46</sup>

$$E(z) = \frac{\int_{-L_z/2}^z \rho_q(z') dz'}{\epsilon_0} \quad (2)$$

where  $\epsilon_0$  is the vacuum permittivity and  $L_z$  is the length of the simulation cell in the  $z$  direction.

## RESULTS AND DISCUSSIONS

**Structural and Electrostatic Properties of Quartz-Supported Neat Lipid Bilayers.** To delineate the underlying differences between model eukaryotic and prokaryotic cell membranes, we analyzed structural and electrostatic properties of hydrated DMPC and mixed DMPC/G bilayers supported on a quartz crystal in the absence of the added peptide. Figure 2 compares mass density distributions of lipid, water, and sodium

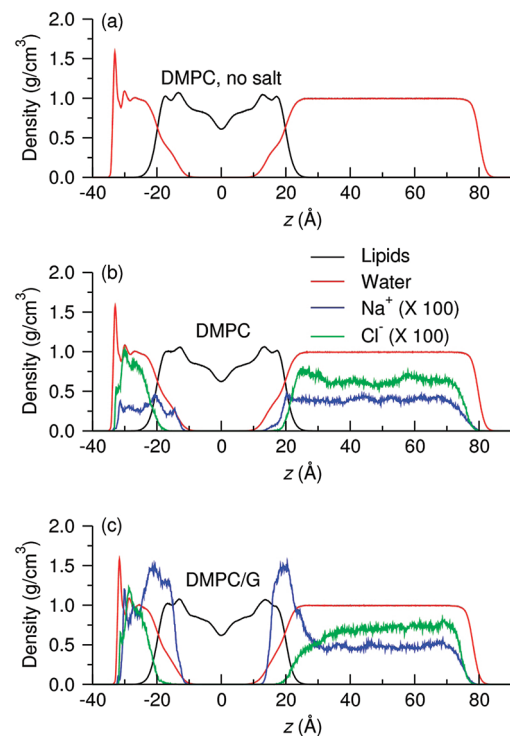


**Figure 2.** Mass density distributions of components of the quartz crystal supported lipid bilayers: (a) DMPC bilayer without salt ions, (b) DMPC bilayer with added salt ions, and (c) DMPC/G bilayer with added salt ions. Black, red, blue, and green lines represent lipid, water, sodium, and chloride, respectively. The  $z$  position in this and subsequent figures is with respect to the membrane center.

and chloride ions in the  $z$  direction normal to the lipid bilayer plane. Density distributions of lipids and water (Figure 2) were all similar regardless of the compositions of lipids and presence or absence of salt ions. However, in the upper bulk water phase at  $z > 0 \text{ \AA}$ , part b and c of Figure 2 show a noticeable difference in sodium ion localization and penetration into the model membranes, with a deeper sodium ion penetration and enhanced density in the DMPC/G lipid bilayer compared to the DMPC bilayer. Chloride ions exhibited the opposite behavior, with enhanced density at the DMPC water interface and decreased density at the DMPC/G water interface. At distances farther away from the interface ( $z > 28 \text{ \AA}$ ), the nearly uniform ion distributions in parts b and c of Figure 2 indicate the limit of the bilayer influence on ion ordering in the solvent phase. The unequal distribution of sodium and chloride ions at the interface resulted in a slight excess of a net system positive charge near the DMPC membrane and a slightly positive electric field of  $0.3 \text{ mV}/\text{\AA}$  in the bulk phase of the upper water layer. Part a of Figure 3 shows both the fluctuations in the total

negative electric field value of  $-0.2 \text{ mV}/\text{\AA}$  in the bulk phase of the upper water layer for the DMPC/G lipid bilayer. This implies a slightly negative net effective charge near the DMPC/G lipid bilayer caused by incomplete shielding of the negative charges of anionic lipids, despite the sodium ion's tendency to penetrate deeper into the membrane. Importantly, in the absence of any salt ions (part a of Figure 2), the average electric field in the bulk phase of water is nearly zero (part a of Figure 3). This confirms that the presence of counterions and physiological salts play a significant role in modulating the electrostatic properties of the lipid bilayer system.

In spite of the fluctuations shown in Figure 3, the electric fields have a non-negligible effect in terms of polarizing the bulk aqueous solution. To characterize this effect, we measured orientational polarization of water by calculating the average value of cosine of the angle between the water dipole and the  $z$ -axis,  $\langle \cos\theta_{\text{dipole},z} \rangle$ . This quantity is a sensitive probe of the local electric field in simulated systems.<sup>28,46,47</sup> Part b of Figure 3 shows  $\langle \cos\theta_{\text{dipole},z} \rangle$  as a function of the  $z$  position for different bilayer systems. In the absence of salt ions, water was not polarized, and  $\langle \cos\theta_{\text{dipole},z} \rangle$  was close to zero in the bulk phase of water with the DMPC bilayer, consistent with the net zero electric field in the bulk phase shown in part a of Figure 3. On the other hand, slightly positive and negative  $\langle \cos\theta_{\text{dipole},z} \rangle$  values were observed for the DMPC and DMPC/G bilayers, respectively, consistent with the electric field profiles in part a of Figure 3. Both the zwitterionic DMPC charges and the negative charges introduced by the anionic DMPG lipids are strongly shielded by the counterions and salts near the lipid bilayer. However, in the presence of salt, the net small polarization of the bulk water results in opposite effects in the two bilayers: in the DMPC system, water dipoles are oriented away from the interface, whereas, in the DMPC/G systems, they are oriented toward the interface. As indicated in part b of Figure 3, this effect is small in magnitude but significant in differentiating the electrostatic behavior of the two systems as it relates to indolicidin adsorption.

**Interaction of Indolicidin with Quartz-Supported Lipid Bilayers.** To investigate the interaction between indolicidin and the model lipid bilayers, we performed a series of simulations where the  $z$  position of indolicidin was restrained at  $1 \text{ \AA}$  intervals from the bulk phase of the upper water layer to the membrane interface. As described in the Methods section, we used five different initial conformations of indolicidin and two different compositions of lipid bilayers to generate results that were independent of starting configuration. Figure 4 shows the resulting PMF profiles combined from the five independent simulations. The placement of indolicidin at the membrane surface was associated with a minimum PMF of  $-3.5 \pm 0.2 \text{ kcal/mol}$  at  $z = 25.0 \text{ \AA}$  for the prokaryotic DMPC/G bilayer, compared to  $-0.6 \pm 0.6 \text{ kcal/mol}$  at  $z = 28.1 \text{ \AA}$  for the eukaryotic DMPC bilayer. Consistent with the electric field profiles and orientational polarization of bulk water shown in Figure 3, indolicidin exhibited a slight attraction to the mixed DMPC/G lipid bilayer but was weakly repulsed by the DMPC bilayer. This difference in the PMF profiles of indolicidin with DMPC and DMPC/G lipid bilayers reflects the selective association of indolicidin with the bacterial cell membrane.

Because the microscopically distance-dependent PMF for indolicidin is not readily available from experiments, we estimated two macroscopic quantities from our simulation data. Applying the formalism from Gray and co-workers,<sup>48,49</sup> we used the distance-dependent PMF in Figure 4 to estimate

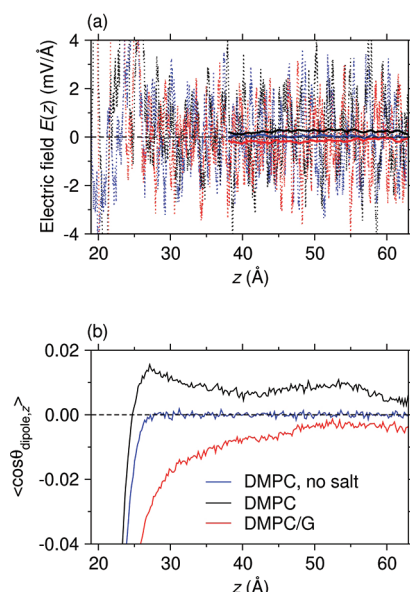


**Figure 3.** Distributions of electric field and water polarization in the upper water layer. Blue lines show results for the DMPC bilayer without salt ions. Black and red lines show results for DMPC and DMPC/G bilayers with added salt ions, respectively. (a) Electric field  $E(z)$  calculated by eq 2. Dotted lines represent raw results, which fluctuate around zero. To capture the trends in these highly fluctuating electric field values, we calculated  $20 \text{ \AA}$  running averages of  $E(z)$  near the bulklike region of the upper water layer shown as solid lines. (b) Orientational polarization of water estimated by  $\langle \cos\theta_{\text{dipole},z} \rangle$ , the average cosine of the angle between the water dipole and the  $z$  axis.

electric field distributions and the smaller but consistently nonzero average electric field values calculated using eq 2. The net positive charge near the model eukaryotic cell membrane in the presence of salt ions can play a role in the selective antimicrobial action by deterring cationic antimicrobial peptides from approaching the bilayer. However, the magnitude of the net effect is small and could be subject to the specifics of the lipid and ions of the particular system modeled. Part c of Figure 2 shows that the additional sodium counterions associated with the anionic lipids are preferentially located near the mixed DMPC/G bilayer. However, the electric field distribution shown in part a of Figure 3 exhibits a slightly

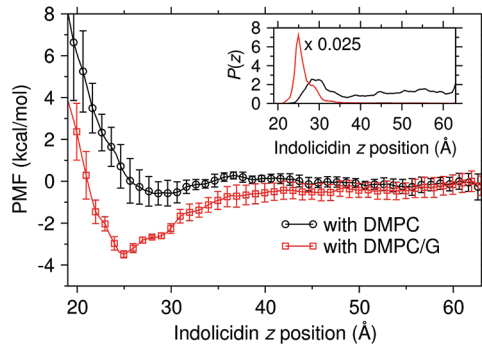


**Figure 4.** Potential of mean force (PMF) or free energy profiles of indolicidin as a function of the distance of the peptide from the membrane center of DMPC and DMPC/G lipid bilayers. PMF distributions with DMPC and DMPC/G lipid bilayers are shown in solid lines with circles and squares, respectively. Errors reported were based on the 95% confidence interval estimated as 1.96 times the standard error. Standard errors were estimated from the analysis of five independent PMF distributions obtained from five sets of simulations with different starting configurations of indolicidin for each bilayer. The insert shows the corresponding probability distribution  $P(z)$  of indolicidin on the two bilayers. The distribution for the DMPC/G bilayer was reduced by a factor of 40 for easier comparison with the DMPC bilayer.

the free energy of indolicidin adsorption ( $\Delta G^\circ$ ) to be  $-1.94 \pm 0.56$  kcal/mol for the model prokaryotic cell membrane and of  $-0.05 \pm 0.46$  kcal/mol for the eukaryotic membrane. From the PMF curve in Figure 4, we further calculated the maximum adsorption binding force to be 21 pN at  $z = 31$  Å and 41 pN at  $z = 30$  Å for the DMPC and DMPC/G bilayers, respectively. The DMPC binding force value was close to the value determined for bovine lactoferricin adsorption on the closely related zwitterionic 1-palmitoyl-2-oleoyl-sn-glycero-3-phosphocholine (POPC) pure bilayer.<sup>48</sup>

To characterize the overall energetic changes as indolicidin approaches the lipid bilayer, we calculated the average potential energy (enthalpy) as a function of a center-of-mass distance of indolicidin from the membrane center. Part a of Figure 5 shows the results for both bilayer systems. The total potential energy of the system decreased, that is, contributed favorably to the free energy of adsorption, as indolicidin approached both types of lipid bilayers. This implies that the approach of indolicidin toward either lipid bilayer was an enthalpically favorable process. Parts b and c of Figure 5 show the further division of the potential energies in terms of electrostatic and van der Waals components, respectively. Counterintuitively, the total electrostatic energies of the system did not depend strongly on distance and was not attractive as indolicidin approached the membrane; in fact, the electrostatic component of the enthalpy became repulsive at closer distances. However, the van der Waals energies decreased significantly as indolicidin moved closer to the lipid bilayers. Part d of Figure 5 shows the distance-dependent profiles of the entropic contribution to the PMF as estimated by  $-T\Delta S = PMF - \Delta U$ . The contribution of the entropic component ( $-T\Delta S$ ) to the free energy of both bilayer/indolicidin systems was opposite the contribution of the enthalpic term. As indolicidin starts interacting more closely with the headgroups of the lipids and penetrating into the outer portion of the bilayer, there is an entropic penalty. The detailed balance between these forces determined the adsorption free energy and the locations of the PMF minima seen in Figure 3. Although the statistical uncertainty of the separated free energy

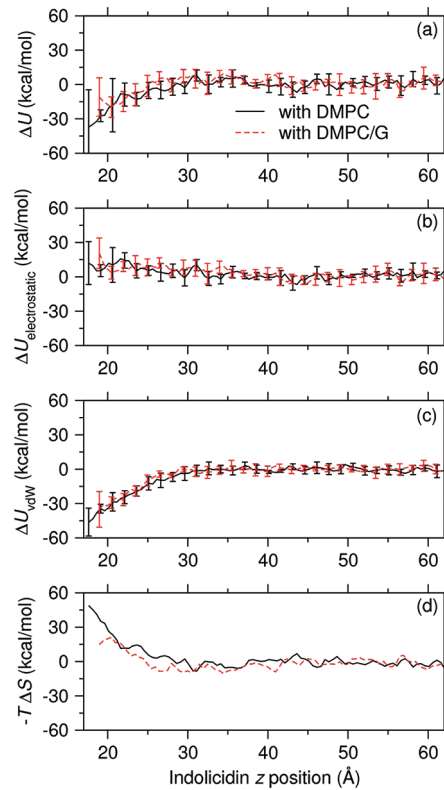


**Figure 5.** Contribution of different energy terms as a function of indolicidin  $z$  position from the membrane center: (a) total potential energy, (b) electrostatic energy, (c) van der Waals energy, and (d) entropic contribution. Solid and dashed lines represent results with DMPC and DMPC/G lipid bilayers, respectively. Errors reported were based on 95% confidence intervals estimated as 1.96 times the standard error. Standard errors were estimated by the analysis of energy values obtained from five sets of simulations with different starting configurations of indolicidin for each bilayer.

components is larger than for the PMF calculation, we estimated the  $\Delta U$  and  $-T\Delta S$  for both bilayer systems at their respective minima to be  $-2$  kcal/mol and  $+1$  kcal/mol for the DMPC bilayer and  $-1$  kcal/mol and  $-2$  kcal/mol for the mixed DMPC/G bilayer. Qualitatively, the enthalpic changes are similar, whereas the entropic terms favor the DMPC/G system. To elucidate the nature of the indolicidin interaction with the bilayers, we next characterized the structural properties tied to these energetic changes.

**Structural Properties of Indolicidin.** We characterized structural properties of indolicidin as a function of its distance to the lipid bilayers. Figure 6 shows snapshots of indolicidin from the simulations at different  $z$  positions with the mixed DMPC/G lipid bilayer. In part a of Figure 6, indolicidin is located in the middle of the upper water layer ( $z = 48.5$  Å from the membrane center). Part b of Figure 6 shows indolicidin at  $z = 34.7$  Å from the membrane center, where two adjacent arginine residues near the C-terminus of indolicidin have begun to interact with the mixed lipid bilayer. Part c of Figure 6 shows indolicidin at  $z = 25.6$  Å, where positively charged lysine and arginine residues interact with the mixed lipid bilayer. Part d of Figure 6 shows indolicidin at  $z = 19.1$  Å, where several hydrophobic tryptophan residues are interacting with the lipid hydrocarbon chains and several of the positively charged residues are making contacts with lipid headgroups in the interfacial region.

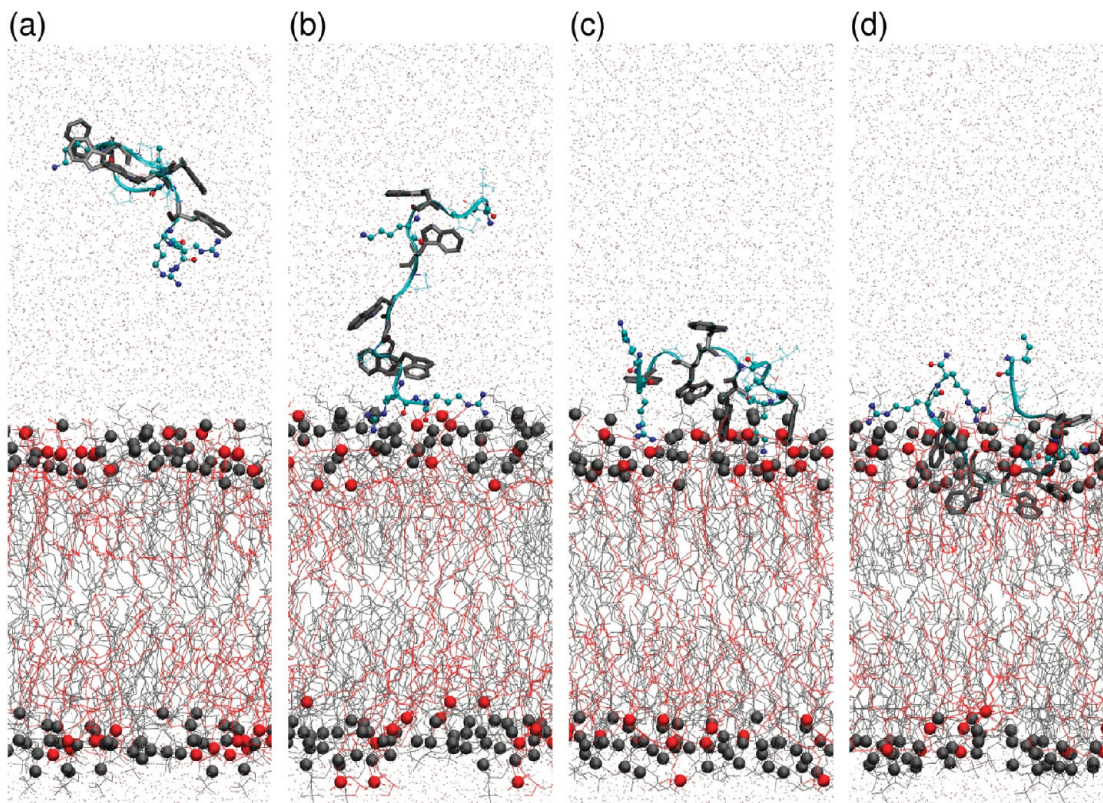


**Figure 6.** Snapshots of indolicidin at (a) 48.5, (b) 34.7, (c) 25.6, and (d) 19.1 Å away from the center of the DMPC/G lipid bilayer. DMPC and DMPG lipids are represented by gray and red lines, respectively. Phosphorus atoms in the headgroups of DMPC and DMPG lipids are shown as gray and red spheres, respectively. Indolicidin is represented by a ribbon in cyan. Non-hydrogen atoms of positively charged lysine and arginine residues and N-terminus are explicitly represented as balls and sticks. Carbon, nitrogen, and oxygen atoms are shown in cyan, blue, and red, respectively. Indole rings of hydrophobic tryptophan residues are represented by thick gray bonds. Oxygen atoms of water molecules are shown as small pink balls.

Part a of Figure 7 shows the distributions of backbone rmsd of indolicidin with respect to the experimental NMR structure averaged over all configurations in the production runs. For both lipid bilayers, the structure of indolicidin deviated significantly from the experimental NMR structure. Part b of Figure 7 shows backbone rmsd of indolicidin as a function of indolicidin *z* position from the membrane center. The average backbone rmsd values of indolicidin in bulk water phase and near the bilayer were similar, whereas indolicidin exposed to the vacuum ( $z > 60$  Å) displayed larger average backbone rmsd values. Part c of Figure 7 shows orientational distributions of indolicidin measured by the average cosine of the angle between the *z* axis and the long axis of indolicidin determined from the inertia tensor ( $\langle \cos\theta_{\text{peptide},z} \rangle$ ). The angle  $\theta_{\text{peptide},z}$  ranged from 0 to 90 degrees with respect to the *z* axis and  $\cos\theta_{\text{peptide},z}$  ranged from 0 (parallel to the membrane interface) to 1 (perpendicular to the membrane interface). When indolicidin was located in the bulk water phase,  $\langle \cos\theta_{\text{peptide},z} \rangle$  was about 0.5, consistent with an isotropic distribution. Near the water/vacuum interface ( $60$  Å  $< z < 70$  Å), indolicidin adopted a perpendicular orientation with respect to the interface. More importantly, however, when indolicidin was located closer to the lipid bilayer,  $\langle \cos\theta_{\text{peptide},z} \rangle$  was slightly increased ( $30$  Å  $< z < 40$  Å) but decreased in region where the minima of the PMF are located (Figure 3). Thus, in the energetically most favorable configurations, indolicidin adopts a roughly parallel orientation with respect to the membrane interface. Part c of Figure 6 shows an example of such a

conformation. The structural variations and orientational preferences of indolicidin were qualitatively similar for both the DMPC and DMPC/G bilayer systems.

Khandelia and Kaznessis<sup>18</sup> observed a persistent cation–π interaction between TRP11 and ARG13 of indolicidin in the zwitterionic DPC micelle. To determine whether we observe a similar stabilizing interaction, we calculated the distributions of the distance between TRP11 and ARG13 of indolicidin near DMPC and DMPC/G lipid bilayers as shown in part d of Figure 7. A larger population of indolicidin with the TRP11-ARG13 distance less than 5 Å was observed near the zwitterionic DMPC bilayer than the mixed DMPC/G bilayer, which is consistent with the simulation results by Khandelia and Kaznessis.<sup>18</sup> However, no persistent cation–π interaction was observed for indolicidin near either lipid bilayer in our simulations.

**Distributions of Positively Charged Residues and Tryptophan Residues.** In Figure 8, we compared distributions of positively charged residues and hydrophobic tryptophan residues from indolicidin adsorbed on DMPC and DMPC/G lipid bilayers. To select the indolicidin interface-contact conformations, we used configurations where the center-of-mass of indolicidin was located between 20 and 27 Å away from the membrane center. Part a of Figure 8 shows that positively charged residues were more preferentially distributed near the headgroups of the DMPC/G lipid bilayers than in the DMPC system. However, part b of Figure 8 shows that there was no significant difference between distributions of

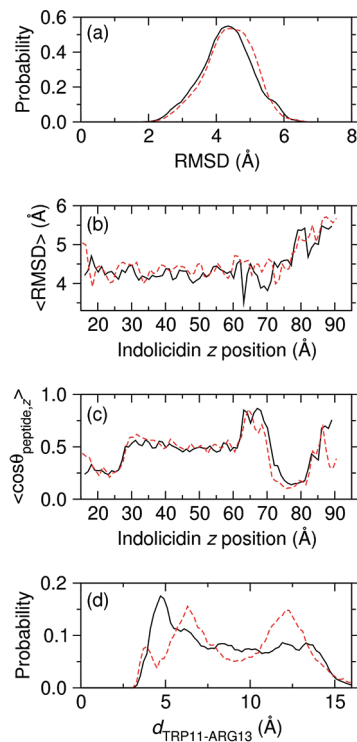


**Figure 7.** Structural properties of indolicidin in the lipid bilayer systems. Solid and dashed lines represent results from simulations with DMPC and DMPC/G lipid bilayers, respectively. Backbone rmsd of indolicidin was calculated with respect to the structure of indolicidin bound to a dodecylphosphocholine micelle as determined by NMR.<sup>8</sup> (a) Distributions of rmsd from all production runs. (b) Average rmsd as a function of indolicidin *z* position from the membrane center. (c) Orientation of indolicidin peptide measured by  $\langle \cos\theta_{\text{peptide},z} \rangle$ , the average cosine of the angle between the peptide long axis and the membrane normal, as a function of indolicidin *z* position. The data for *z* > 60 Å corresponds to indolicidin near the water/vacuum interface centered around *z* = 80 Å. (d) Distributions of the distance between TRP11 and ARG13 of indolicidin near DMPC and DMPC/G lipid bilayers. The distance between TRP11 and ARG13 ( $d_{\text{TRP11-ARG13}}$ ) was defined as the distance between the CE2 atom of the tryptophan indole ring and the CZ atom of arginine as defined in the PDB file. The distributions were calculated with the conformations of indolicidin whose *z* position is between 20 Å and 27 Å away from the membrane center.

tryptophan residues near the DMPC and DMPC/G lipid bilayers. The primarily hydrophobic interactions stemming from tryptophan/lipid contacts were roughly similar in nature, commensurate with the similar enthalpic profiles shown in Figure 5 for both types of bilayers. Thus, the distinction between the two bilayers in terms of interactions lies primarily in how the positively charged residues are distributed in the interface region of the bilayer and how the system of solvent and ion molecules accommodate these configurations. Given that the enthalpic component derived from electrostatic interactions between the two systems is not that different due to charge conservation and counterion shielding, the conformations underlying both distributions in part a of Figure 8 are enthalpically equivalent. The difference in density of positively charged residues located in the bilayer headgroup region around *z* = 20 Å in part a of Figure 8 instead points to a mechanism whereby positively charged ions normally associated with the bilayer are replaced by positive charges from indolicidin. This type of an effect would essentially be

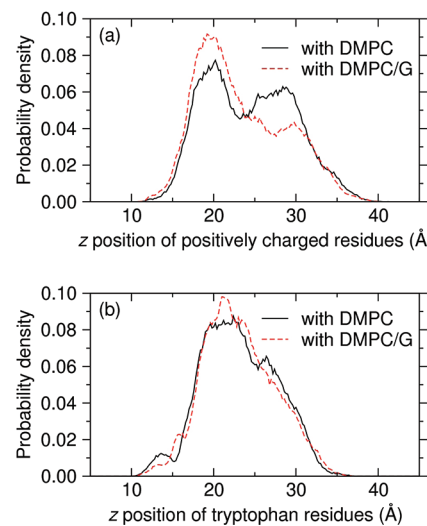


**Figure 8.** Distributions of positively charged residues and hydrophobic tryptophan residues. Distributions were calculated from configurations where indolicidin was located between 20 and 27 Å away from the membrane center. (a) Distributions of positively charged residues were estimated as the sum of density distributions of the N atom at the N-terminus, the NZ atom of lysine, and the CZ atom of arginine as defined in the PDB file. (b) Distributions of tryptophan residues calculated by the density distribution of the CE2 atom of the indole ring in the PDB file.

enthalpically neutral but entropically favorable. This interpretation is consistent with the observed difference in entropy changes seen for the two different bilayers.

These results indicate that the electrostatic interactions between positively charged residues of indolicidin and the headgroups of anionic lipids in the mixed lipid bilayer underlie the specificity, but not the strength of attraction, of indolicidin toward the bacterial cell membrane. Instead, the increased strength of adsorption free energy in the DMPC/G model prokaryotic membrane versus the DMPC eukaryotic membrane is postulated to be derived from a gain in entropy due to counterion release.<sup>49,50</sup> Figure 9 shows the positive charge distribution in both bilayer systems, both in the presence and absence of indolicidin at the bilayer surface. Part a of Figure 9 shows that the total charge distribution seen in the neat system has been replaced by a combination of indolicidin charges and Na<sup>+</sup> atoms for the DMPC/G bilayer. Consequently, sodium atoms strongly localized to the surface in the absence of indolicidin were released into the bulk solution upon surface adsorption of indolicidin, providing a relative gain in entropy. For the DMPC bilayer however, parts b and c of Figure 2 show that the sodium atoms in the neat solution are not strongly localized to the bilayer surface compared to the bulk solution. Consequently, although adsorption of indolicidin at the surface also released sodium atoms, it did not provide the same relative gain in entropy as for the DMPC/G bilayer. The observed entropy change is an intrinsic property of the entire system and cannot strictly be decomposed into atomic components. However, in support of our interpretation, Vivcharuk and Kaznessis<sup>50</sup> found the peptide–membrane attraction to be dominated by the entropy increase due to the release of counterions in a POPG/POPE lipid bilayer with MD simulations where orientations and conformations of the peptide were constrained.

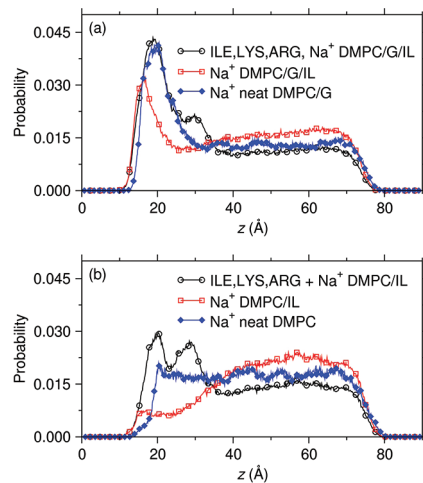


**Figure 9.** Distributions of  $\text{Na}^+$  and positively charged residues in the presence and absence of indolicidin. Distributions for the systems with indolicidin adsorbed onto the bilayer were calculated from configurations where the peptide was located between 20 and 27 Å away from the membrane center. The contribution from the positive charged residues of indolicidin was calculated as the sum of density distributions of the N atom at the N-terminus, the NZ atom of lysine, and the CZ atom of arginine as defined in the PDB file. (a) The total positive charge distribution for the DMPC/G bilayer including  $\text{Na}^+$  and indolicidin charges (Ile, Lys, Arg,  $\text{Na}^+$  DMPC/G/IL), the charge distribution due to  $\text{Na}^+$  only in the presence of indolicidin ( $\text{Na}^+$  DMPC/G/IL), and the charge distribution due to  $\text{Na}^+$  in the neat systems taken from Figure 2 ( $\text{Na}^+$  neat DMPC/G). (b) The same distributions for the DMPC bilayer.

**Bilayer Perturbations and Lipid Order Parameters.** Lastly, we examined the lipid bilayer itself for structural features that could differentiate the response of the bilayers to indolicidin adsorption. We created profiles of the lipid order parameter  $-S_{CD}$  along the lipid acyl chain for DMPC and DMPC/G bilayers using eq 1. We constructed  $-S_{CD}$  profiles for phospholipids that were in contact with indolicidin and compared them with  $-S_{CD}$  profiles obtained when the peptide was sufficiently distant ( $z > 50$  Å from the membrane center) such that no peptide–phospholipid contact existed. A lipid molecule in the upper leaflet of the bilayer was considered in contact with the peptide if the center-of-mass  $z$  position of indolicidin was between 20 and 27 Å away from the membrane center and the radial distance of the phosphorus atom of the lipid from the cylindrical axis along the  $z$  direction that passes through the center-of-mass position of peptide was within 8 Å. Parts a and b of Figure 10 show the calculated  $-S_{CD}$  profiles for the DMPC and DMPC/G bilayers, respectively. For  $-S_{CD}$  profiles without the peptide–lipid contact, the profiles combined from both upper and lower leaflets of lipid bilayers are shown. We did not observe any significant difference between  $-S_{CD}$  profiles calculated separately for upper and lower leaflets of bilayers (data not shown). This indicates that the effect of the quartz solid support on the structural properties of the lipid bilayer was negligible when there was a thick water layer between the quartz surface and the lipid bilayer as we observed in our previous study.<sup>28</sup> As expected,  $-S_{CD}$  values from lipids in contact with the peptide were smaller than lipids not in contact, indicating a more disordered acyl chain for lipids in contact with indolicidin. The average  $z$  displacements of the phosphorus atoms of lipids in contact with the peptide from those of upper-leaflet lipids not in contact

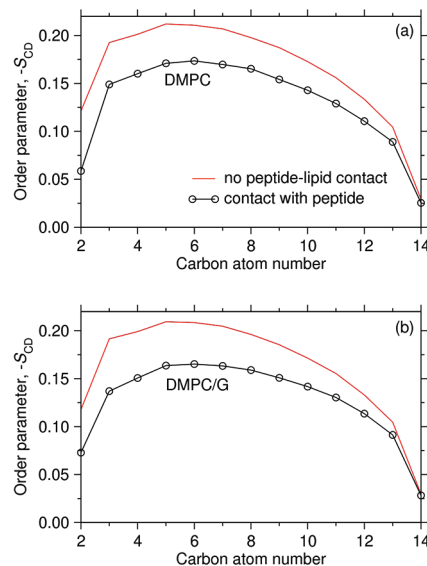


**Figure 10.** Order parameter  $-S_{CD}$  along the lipid acyl chain of (a) DMPC and (b) DMPC/G bilayers calculated with eq 1. The carbon atoms are numbered sequentially from head to tail regions of a lipid. Order parameters for lipids with and without the peptide–lipid contact are represented by lines with and without circles, respectively.

with the peptide were  $-1.69$  and  $-2.0$  Å for DMPC and DMPC/G bilayers, respectively. Even though  $-S_{CD}$  values for carbon numbers 3 through 9 near the lipid headgroup in the DMPC/G bilayer decreased slightly more than those for the DMPC bilayer in contact with the peptide, we found no significant difference in changes in  $-S_{CD}$  profiles between DMPC and DMPC/G lipid bilayers.

## SUMMARY AND CONCLUSIONS

In this study, we characterized the interaction of the antimicrobial peptide indolicidin with solid-supported model bacterial and eukaryotic cell membranes. We based our study on extensive all-atom molecular dynamics simulations combined with rigorous treatment of the electrostatic boundary condition to derive structural and energetic insights. The calculated free energy profiles of indolicidin in proximity to model bacterial and eukaryotic cell membranes revealed that there was a preferential attraction to the bacterial cell membrane. Placement of indolicidin at the membrane surface was associated with a minimum PMF of  $-3.5 \pm 0.2$  kcal/mol at the prokaryotic membrane, compared to  $-0.6 \pm 0.6$  kcal/mol at the eukaryotic membrane. We calculated the free energy of adsorption ( $\Delta G^\circ$ ) from the PMF distance profile to be  $-1.94 \pm 0.56$  kcal/mol for the model prokaryotic cell membrane and  $-0.05 \pm 0.46$  kcal/mol for the model eukaryotic membrane. We also observed that indolicidin was preferentially located near the membrane interface lying parallel to the interface in agreement with previous experimental and computational studies.

We analyzed the energetic components and the structural changes for both types of bilayers to gain insights into the nature of indolicidin adsorption. Although we cannot fully address all possible lytic mechanisms indolicidin is engaged in, the initial association of the peptide with prokaryotic membranes is a required step for biological activity. We found that the effect of counterions and salts at physiological concentrations minimized the direct electrostatic component of

the enthalpic contributions to the PMF. Instead, indolicidin derived the bulk attractive force from van der Waals interactions. This attractive force was counteracted by entropic penalties as the indolicidin molecule approached the bilayer interface from the solution. These effects were roughly similar for both model membranes systems, but with one important difference. The preferential placement of the positively charged residues close to lipid headgroups of the DMPC/G bilayer as opposed to the DMPC bilayer allowed more counterions to be released into the bulk aqueous solution, resulting in a reduced entropic penalty.

In the current study, we investigated adsorption of a single indolicidin molecule on to the bilayer. We fixed the simulation box sizes in directions parallel to the membrane/water interface to maintain the geometry of the quartz (011) surface. For a broader understanding of membrane perturbations at deeper penetrations and higher concentrations<sup>51</sup> of indolicidin, as well as other antimicrobial peptide classes, we would require a flexible simulation cell that can accommodate larger rearrangement of the bilayer than seen here. We are currently developing a constant pressure simulation methodology to accommodate larger lipid bilayer perturbations due to antimicrobial peptides.

In summary, the nature of the indolicidin surface adsorption depended on an electrostatic guiding component, an attractive enthalpic component derived from van der Waals interactions, and an entropic factor dependent on the amount of counterion release from the bilayer surface. Commensurate with this view, introducing additional charged residues into indolicidin will not greatly alter the strength of adsorption but could alter the type of bilayer the peptide would adsorb on.<sup>17</sup> It also follows that modulating the overall van der Waals interactions by substituting the bulkier tryptophan residues with smaller phenylalanine residues will, however, noticeably decrease the adsorption free energy.<sup>17</sup> Engineering indolicidin-based or other cationic peptides based on maintaining or improving the differential surface adsorption profile between eukaryotic and prokaryotic membranes should utilize these principles, whereas the specifics of improving bacterial lysis and reducing hemolytic activity could be guided by different principles.

## AUTHOR INFORMATION

### Corresponding Author

\*Phone: (301) 619-0702, Fax: (301) 619-1983, E-mail: icy@bioanalysis.org.

### Notes

The authors declare no competing financial interest.

## ACKNOWLEDGMENTS

This project was funded in part by a competitive In-house Laboratory Independent Research (ILIR) grant by the U.S. Army Assistant Secretary of the Army for Acquisition, Logistics, and Technology (ASAALT). Funding support for this work also came from the Department of Defense (DoD) High Performance Computing (HPC) Modernization Program Office, under the HPC Software Applications Institute initiative, the U.S. Army Medical Research and Materiel Command. Computational time was provided by the U.S. Army Research Laboratory, U.S. Army Engineer Research and Development Center, and Navy DoD Supercomputing Resource Centers. The opinions or assertions contained herein are the private views of the authors and are not to be construed

as official or as reflecting the views of the U.S. Army or of the U.S. Department of Defense.

## REFERENCES

- (1) Zasloff, M. *Nature* **2002**, *415*, 389–395.
- (2) Yeaman, M. R.; Yount, N. Y. *Pharmacol. Rev.* **2003**, *55*, 27–55.
- (3) Brogden, K. A. *Nat. Rev. Microbiol.* **2005**, *3*, 238–250.
- (4) Hancock, R. E. W. *Lancet* **1997**, *349*, 418–422.
- (5) Hancock, R. E. W.; Lehrer, R. *Trends Biotechnol.* **1998**, *16*, 82–88.
- (6) Hancock, R. E. W.; Sahl, H. G. *Nat. Biotechnol.* **2006**, *24*, 1551–1557.
- (7) Selsted, M. E.; Novotny, M. J.; Morris, W. L.; Tang, Y. Q.; Smith, W.; Cullor, J. S. *J. Biol. Chem.* **1992**, *267*, 4292–4295.
- (8) Rozek, A.; Friedrich, C. L.; Hancock, R. E. W. *Biochemistry* **2000**, *39*, 15765–15774.
- (9) Falla, T. J.; Karunaratne, D. N.; Hancock, R. E. W. *J. Biol. Chem.* **1996**, *271*, 19298–19303.
- (10) Ladokhin, A. S.; Selsted, M. E.; White, S. H. *Biophys. J.* **1997**, *72*, 794–805.
- (11) Bahng, M. K.; Cho, N. J.; Park, J. S.; Kim, K. *Langmuir* **1998**, *14*, 463–470.
- (12) Ha, T. H.; Kim, C. H.; Park, J. S.; Kim, K. *Langmuir* **2000**, *16*, 871–875.
- (13) Zhang, L. J.; Rozek, A.; Hancock, R. E. W. *J. Biol. Chem.* **2001**, *276*, 35714–35722.
- (14) Shaw, J. E.; Alattia, J. R.; Verity, J. E.; Prive, G. G.; Yip, C. M. *J. Struct. Biol.* **2006**, *154*, 42–58.
- (15) Shaw, J. E.; Epand, R. F.; Hsu, J. C. Y.; Mo, G. C. H.; Epand, R. M.; Yip, C. M. *J. Struct. Biol.* **2008**, *162*, 121–138.
- (16) Askou, H. J.; Jakobsen, R. N.; Fojan, P. *J. Nanosci. Nanotechnol.* **2008**, *8*, 4360–4369.
- (17) Andrushchenko, V. V.; Aarabi, M. H.; Nguyen, L. T.; Prenner, E. J.; Vogel, H. J. *Biochim. Biophys. Acta-Biomembr.* **2008**, *1778*, 1004–1014.
- (18) Khandelia, H.; Kaznessis, Y. N. *J. Phys. Chem. B* **2007**, *111*, 242–250.
- (19) Hsu, J. C. Y.; Yip, C. M. *Biophys. J.* **2007**, *92*, L100–L102.
- (20) Tsai, C. W.; Hsu, N. Y.; Wang, C. H.; Lu, C. Y.; Chang, Y.; Tsai, H. H. G.; Ruaan, R. C. *J. Mol. Biol.* **2009**, *392*, 837–854.
- (21) Mechler, A.; Praporski, S.; Atmuri, K.; Boland, M.; Separovic, F.; Martin, L. L. *Biophys. J.* **2007**, *93*, 3907–3916.
- (22) Chen, X. Y.; Chen, Z. *Biochim. Biophys. Acta-Biomembr.* **2006**, *1758*, 1257–1273.
- (23) Avery, C. W.; Som, A.; Xu, Y. J.; Tew, G. N.; Chen, Z. *Anal. Chem.* **2009**, *81*, 8365–8372.
- (24) Heine, D. R.; Rammohan, A. R.; Balakrishnan, J. *Mol. Simul.* **2007**, *33*, 391–397.
- (25) Roark, M.; Feller, S. E. *Langmuir* **2008**, *24*, 12469–12473.
- (26) Xing, C. Y.; Faller, R. *J. Phys. Chem. B* **2008**, *112*, 7086–7094.
- (27) Hoopes, M. I.; Xing, C.; Faller, R. In *Biomembrane Frontiers*; Faller, R., Longo, M. L., Risbud, S. H., Jue, T., Eds.; Humana Press: New York, 2009; p 101–120.
- (28) Yeh, I. C.; Wallqvist, A. *J. Chem. Phys.* **2011**, *134*, 055109.
- (29) Skarnes, R. C.; Watson, D. W. *Bacteriol. Rev.* **1957**, *21*, 273–294.
- (30) Roux, B. *Comput. Phys. Commun.* **1995**, *91*, 275–282.
- (31) Kale, L.; Skeel, R.; Bhandarkar, M.; Brunner, R.; Gursoy, A.; Krawetz, N.; Phillips, J.; Shinozaki, A.; Varadarajan, K.; Schulten, K. *J. Comput. Phys.* **1999**, *151*, 283–312.
- (32) MacKerell, A. D.; Bashford, D.; Bellott, M.; Dunbrack, R. L.; Evanseck, J. D.; Field, M. J.; Fischer, S.; Gao, J.; Guo, H.; Ha, S.; Joseph-McCarthy, D.; Kuchnir, L.; Kuczera, K.; Lau, F. T. K.; Mattos, C.; Michnick, S.; Ngo, T.; Nguyen, D. T.; Prodhom, B.; Reiher, W. E.; Roux, B.; Schlenkrich, M.; Smith, J. C.; Stote, R.; Straub, J.; Watanabe, M.; Wiorkiewicz-Kuczera, J.; Yin, D.; Karplus, M. *J. Phys. Chem. B* **1998**, *102*, 3586–3616.
- (33) Jorgensen, W. L.; Chandrasekhar, J.; Madura, J. D.; Impey, R. W.; Klein, M. L. *J. Chem. Phys.* **1983**, *79*, 926–935.
- (34) Lopes, P. E. M.; Murashov, V.; Tazi, M.; Demchuk, E.; MacKerell, A. D. *J. Phys. Chem. B* **2006**, *110*, 2782–2792.

- (35) Essmann, U.; Perera, L.; Berkowitz, M. L.; Darden, T.; Lee, H.; Pedersen, L. G. *J. Chem. Phys.* **1995**, *103*, 8577–8593.
- (36) Yeh, I.-C.; Berkowitz, M. L. *J. Chem. Phys.* **1999**, *111*, 3155–3162.
- (37) Ryckaert, J. P.; Ciccotti, G.; Berendsen, H. J. C. *J. Comput. Phys.* **1977**, *23*, 327–341.
- (38) Yeh, I. C.; Wallqvist, A. *J. Phys. Chem. B* **2009**, *113*, 12382–12390.
- (39) Jo, S.; Kim, T.; Iyer, V. G.; Im, W. *J. Comput. Chem.* **2008**, *29*, 1859–1865.
- (40) Petrache, H. I.; Dodd, S. W.; Brown, M. F. *Biophys. J.* **2000**, *79*, 3172–3192.
- (41) Ripoll, D. R.; Liwo, A.; Czaplewski, C.; Scheraga, H. A. *T.A.S.K. Quarterly* **1999**, *3*, 313–331.
- (42) Nemethy, G.; Gibson, K. D.; Palmer, K. A.; Yoon, C. N.; Paterlini, G.; Zagari, A.; Rumsey, S.; Scheraga, H. A. *J. Phys. Chem.* **1992**, *96*, 6472–6484.
- (43) Kumar, S.; Bouzida, D.; Swendsen, R. H.; Kollman, P. A.; Rosenberg, J. M. *J. Comput. Chem.* **1992**, *13*, 1011–1021.
- (44) Gallicchio, E.; Andrec, M.; Felts, A. K.; Levy, R. M. *J. Phys. Chem. B* **2005**, *109*, 6722–6731.
- (45) Vermeer, L. S.; de Groot, B. L.; Reat, V.; Milon, A.; Czaplicki, J. *Eur. Biophys. J.* **2007**, *36*, 919–931.
- (46) Yeh, I.-C.; Berkowitz, M. L. *J. Chem. Phys.* **1999**, *110*, 7935–7942.
- (47) Yeh, I.-C.; Hummer, G. *Biophys. J.* **2004**, *86*, 681–689.
- (48) Vivcharuk, V.; Tomberli, B.; Tolokh, I. S.; Gray, C. G. *Phys. Rev. E* **2008**, *77*, 11.
- (49) Tolokh, I. S.; Vivcharuk, V.; Tomberli, B.; Gray, C. G. *Phys. Rev. E* **2009**, *80*, 12.
- (50) Vivcharuk, V.; Kaznessis, Y. *J. Phys. Chem. B* **2010**, *114*, 2790–2797.
- (51) Woo, H. J.; Wallqvist, A. *J. Phys. Chem. B* **2011**, *115*, 8122–8129.